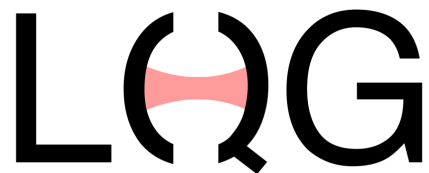




ÉCOLE POLYTECHNIQUE FÉDÉRALE DE LAUSANNE



LABORATORY FOR QUANTUM GASES

SIMPLE HIGH-STABILITY TRANSFER AND FILTER CAVITY FOR CAVITY QED WITH QUANTUM GASES

SPECIALIZATION SEMESTER REPORT

Supervised by: Timo Zwettler, Prof. Jean-Philippe Brantut

Zeyang Xue

January 10, 2024

Abstract

This manuscript reports the second generation transfer cavity used in the laser and cavity stabilization chain. The first generation transfer cavity has a very high finesse of 3×10^4 at 671 nm. However, it also has two drawbacks: low cavity transmission and a lack of thermal stability[1]. The new design of the cavity addresses these problems. The new cavity features a finesse of 5×10^3 , which corresponds to a cavity linewidth below 250 kHz at 1064 nm given the cavity length of 135 mm. The cavity transmission reaches above 50% to be utilised as a passive frequency filter cavity. Temperature regulation and low thermal expansion material are applied to the cavity. The thermal expansion coefficient of the cavity is $1.6 \times 10^{-6} / ^\circ\text{C}$. The new cavity will be installed to the quantum gas experiment to improve the thermal stability of the stabilization chain. The simplicity and cost-effectiveness make it a perfect tool for the future experiments.

1 Introduction

1.1 The Cavity QED with Quantum Gases Experiment

Cavity quantum electrodynamics (QED) is of great interest of quantum science and technology today. Our cavity QED quantum gas experiment combines a strongly-correlated Fermi gas with cavity QED[2], which allows us to explore the interplay of short-range collisional interactions with cavity-mediated long-range interactions[3, 4].

In the heart of our cavity QED quantum gas experiment is the science cavity. The science cavity confines two lasers[2]:

- The 1064 nm Lock/Trap laser, which is precisely on-resonance to the science cavity.
- The 671 nm Probe/Pump laser, which has independently tunable detunings with respect to both the science cavity resonance and the $2s$ to $2p$ transition of ${}^6\text{Li}$ atoms.

The laser and cavity resonant conditions above requires a smart stabilization scheme, which will be introduced in the next section.

1.2 The Cavity Stabilization Scheme

The canonical experimental method for locking a cavity to a laser is the Pound-Drever-Hall (PDH) technique[5] (see section 2.3).

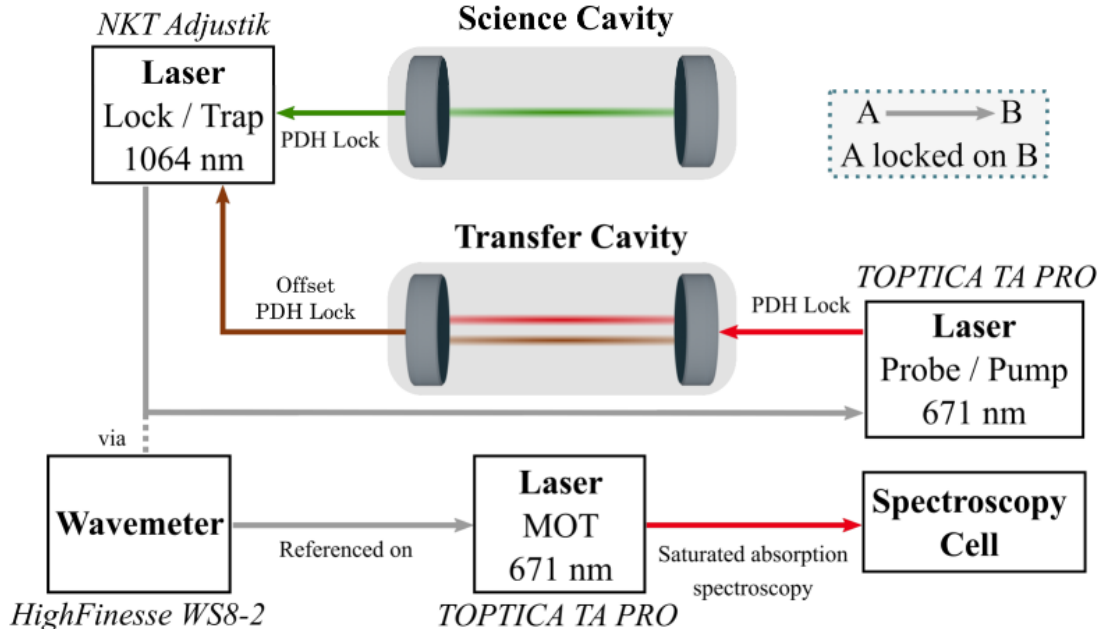


Figure 1: Schematic of the stabilization chain. We only show the laser beams that are involved in the stabilization chain. Arrows in color represents PDH locking or saturated absorption spectroscopy where the directions of the arrows indicate the hierarchy of the chain. Grey arrows showing that the 1064 nm laser is stabilized by referencing the 671 nm laser to the calibrated wavemeter. Cited from [6] with modification.

The absolute reference in the stabilization chain is the spectroscopy cell. The HighFinesse WS8-2 wavemeter is real-time absolutely calibrated by the saturated absorption spectroscopy.

We want to control the detuning of the 671 nm laser from the science cavity. For this we have to ensure the frequency stability between the 1064 nm laser and the 671 nm laser since the science cavity is locked to the 1064 nm laser. This frequency stability transfer is provided by the transfer cavity.

The 671 nm laser is locked to the transfer cavity. The transfer cavity is locked to the 1064 nm laser with a frequency offset ν' . To achieve the offset locking, the 1064 nm laser is modulated at frequency ν' , which generates two sidebands separated from the carrier by a frequency $\pm\nu'$ on the two sides. The transfer cavity fixes the frequency ratio of the 671 nm laser and the sideband of the 1064 nm laser, which is the ratio of the order of the longitudinal cavity mode of the 671 nm laser and the sideband of the 1064 nm Laser. Assuming that the 671 nm laser frequency is ν_P and the 1064 nm laser frequency is ν_L , the above locking implies:

$$\frac{\nu_L \pm \nu'}{\nu_P} = \text{Const.} \approx \frac{671}{1064} \quad (1)$$

where the sign depends on the left or right sideband are used for offset locking.

With the help of the transfer cavity, ν_P is tuned according to ν_L . We apply a digital feedback loop on the 1064 nm laser frequency ν_L such that the 671 nm laser frequency ν_P , measured by the wavemeter, equals to the preset frequency which has the desired detuning to the $2s$ to $2p$ transition of ${}^6\text{Li}$ atom.

The last step in the stabilization chain is to lock the science cavity to the 1064 nm laser. We first double the frequency of the 1064 nm laser to obtain a 532 nm laser. Then lock the 532 nm laser to the science cavity, which ensures the 1064 nm laser to also be resonant with the science cavity.

After all the frequency lockings, the above locking scheme allows to scan the 671 nm laser with respect to the science cavity resonance. Since ν_P is a constant, the transfer cavity fixes the 1064 nm laser sideband frequency $\nu_L \pm \nu'$ to be a constant. By scanning the offset frequency ν' , the 1064 nm laser frequency ν_L and the length of the science cavity are scanning accordingly. Therefore, by scanning the length of the science cavity, the detuning of the 671 nm laser to the science cavity is independently tunable.

1.3 Updates of the Transfer Cavity

This project is building the second generation transfer cavity for the cavity QED experiment. It is aiming for two major updates compared with the first generation transfer cavity[1].

The second generation transfer cavity will be used as a passive filter cavity in the experiment. The filter cavity usually has a high cavity transmission of at least 50%. The first generation transfer cavity has a very high finesse but the transmission is low due to the cavity mirror loss. In the experiment, the transfer cavity linewidth is only required to be below 1 MHz, which is much smaller than the typical detunings used in the experiment. For the second generation transfer cavity, we selected mirrors with lower loss to ensure the high cavity transmission while the transfer cavity linewidth still maintains sufficiently sharp for the stabilization chain.

The second generation transfer cavity is equipped with active temperature controller and two foil heaters. The whole cavity body is made of carbon-fiber-reinforced polymers (CFRP), which has low thermal expansion coefficient. The above updates minimize the cavity length fluctuation due to the change in the room temperature. The stainless steel is used for the new cavity mirror holder replacing the Teflon pieces as the stainless steel has much higher stiffness than the Teflon at high room temperature. The high stiffness of the cavity mirror holder allows a faster feedback bandwidth in the stabilization chain.

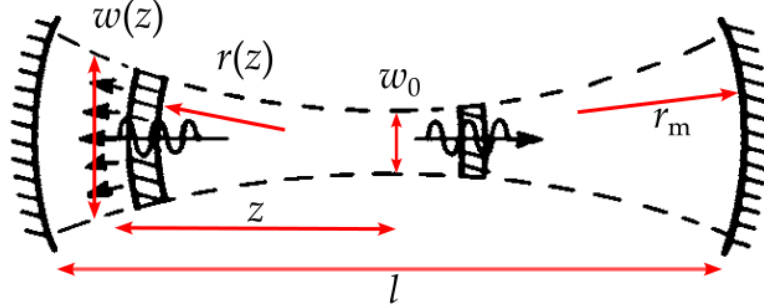


Figure 2: A Gaussian cavity mode confined by two identical concave mirrors. The cavity length l and the curvature of the mirrors r_m are shown in the figure. The two dashed curve show the contour of beam width as a function of the position z . The minimum beam width is w_0 at the center of the cavity. As the wave propagates, the beam width $w(z)$ increases. At the surface of the mirrors, the wavefront curvature of the Gaussian beam coincides with the curvature of the mirrors.

2 Theory of Fabry-Perot Cavity

2.1 The Spectrum of Fabry-Perot Cavity

We build a Fabry-Perot cavity that consists of two mirrors facing each other. The property of a Fabry-Perot cavity can be described in a classical model[7]. For a symmetric cavity where the two cavity mirrors are identical, we assume that the intensity transmission and reflection rate of the two mirrors is T and R , respectively. For a lossless mirror that implies: $T + R = 1$. We further assume the length of the cavity is l and the cavity medium is lossless. The intensity transmission rate $T_{\text{cav}}(\nu)$ of the cavity is given by[7]:

$$T_{\text{cav}}(\nu) = \frac{P_t}{P_{\text{in}}} = \frac{T^2}{(1 - R)^2 + 4R \sin^2(2\pi\nu l/c)} \quad (2)$$

where P_{in} and P_t are the cavity input and transmitted power, respectively. ν is the cavity field frequency and c is the speed of the light.

The intensity transmission rate is a periodic function of ν for a fixed cavity length. The transmission rate reaches its maxima when $2\nu l/c$ is an integer. The cavity field constructively interfere with itself after a round trip in the cavity.

The free spectral range ν_{FSR} is defined as the period of the intensity transmission rate, given by:

$$\nu_{\text{FSR}} = \frac{c}{2l} \quad (3)$$

For high reflectivity mirrors, the reflection rate satisfied: $1 - R \ll 1$. $T_{\text{cav}}(\nu)$ is non-zero if and only if $2\nu l/c$ is close to an integer. For integer k , we define $\Delta\nu$ and ν_k , such that:

$$\nu_k = \frac{kc}{2l} \quad (4)$$

$$\Delta\nu = \nu - \nu_k \quad (5)$$

At the vicinity of ν_k , if $\Delta\nu l/c \ll 1$, we can expand $T_{\text{cav}}(\nu)$ as:

$$T_{\text{cav}}(\nu) = \frac{T^2}{(1 - R)^2 + 4R(\frac{2\pi\Delta\nu l}{c})^2} \quad (6)$$

The transmission spectrum is Lorentzian with linewidth Γ_c , defined as the full-width half-maximum (FWHM), given by:

$$\Gamma_c = \frac{1-R}{\sqrt{R}} \frac{c}{2\pi l} \quad (7)$$

The finesse F of the cavity, defined as the ratio of the linewidth to the free spectral range, is given by:

$$F = \frac{\nu_{\text{FSR}}}{\Gamma_c} = \frac{\pi\sqrt{R}}{1-R} \quad (8)$$

which is solely a function of the intensity reflectivity R .

2.2 Cavity Modes in the Fabry-Perot Cavity

A Fabry-Perot cavity has to satisfy certain cavity stability condition to successfully confine cavity modes. In our experiment, we apply two concave mirrors to trap the TEM₀₀ Gaussian cavity mode, which is the fundamental mode of the cavity[8]. Assuming the beam is propagating along the z -direction with wavevector k and amplitude \vec{E}_0 , the electric field of TEM₀₀ mode is given by the following equation:

$$\vec{E}_{00}(\rho, z) = \vec{E}_0 \frac{w_0}{w(z)} \exp\left(-\frac{\rho^2}{w(z)^2}\right) \exp\left(-ik\left(z + \frac{\rho^2}{2r(z)}\right) + i\psi(z)\right) \quad (9)$$

where w_0 is the beam waist radius. $w(z)$, $r(z)$, and $\psi(z)$ are the beam width, wavefront curvature, and Gouy phase, respectively. They are given by:

$$w(z) = w_0 \sqrt{1 + \left(\frac{z}{z_R}\right)^2} \quad (10)$$

$$r(z) = z + \frac{z_R^2}{z} \quad (11)$$

$$\psi(z) = \arctan\left(\frac{z}{z_R}\right) \quad (12)$$

$$z_R = \frac{1}{2}kw_0^2 \quad (13)$$

where z_R is the Rayleigh length.

To successfully confine the Gaussian mode above, the wavefront curvature at the mirror surface equals to the mirror curvature:

$$r_m = \frac{l}{2} + \frac{2z_R^2}{l} \quad (14)$$

For such a Gaussian beam to exist, it requires the stability condition: $l < 2r_m$.

In addition to the TEM₀₀ fundamental modes, a cavity also supports different high-order transversal modes[7]. The Hermite-Gaussian modes dominate in the experiment in most of the cases as the rotational symmetry is usually broken. The electric field distribution for Hermite-Gaussian modes, labeled by TEM _{m,n} , are given by:

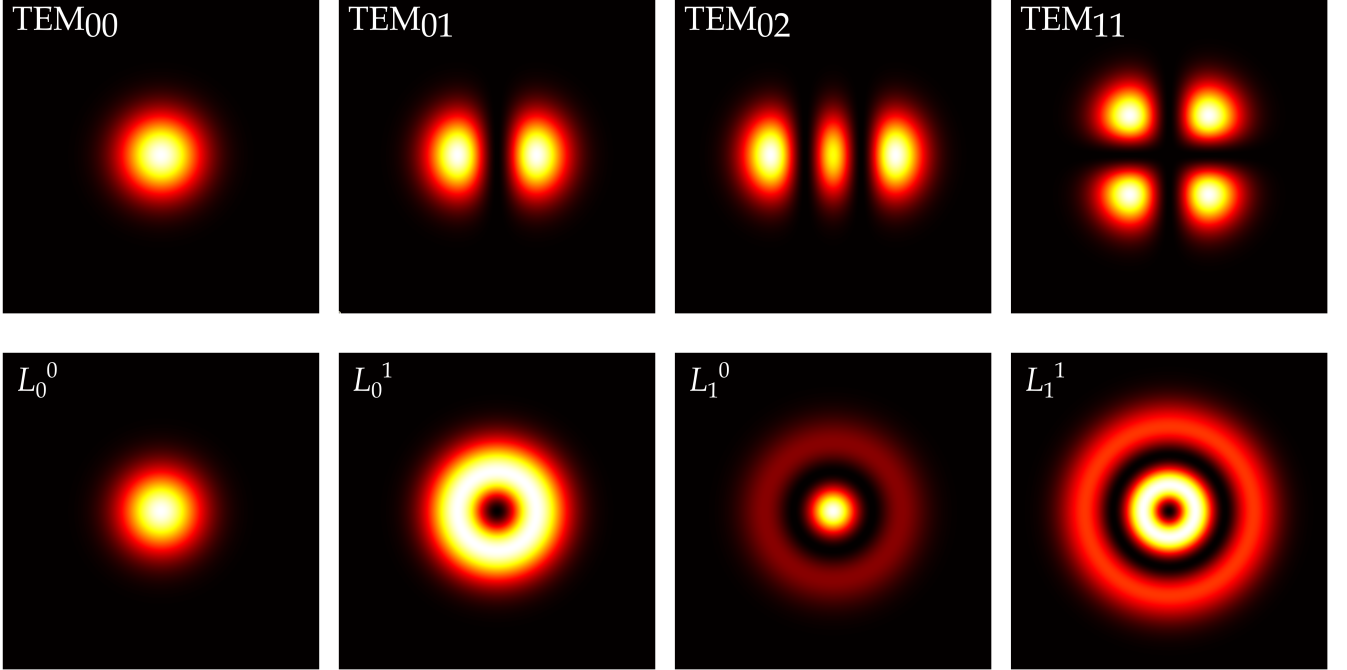


Figure 3: The intensity distributions of the 4 lowest Hermite-Gaussian modes (first row) and Laguerre-Gaussian modes (second row). The lowest TEM_{00} Hermite-Gaussian mode and L_0^0 Laguerre-Gaussian mode, which are identical, are the desired Gaussian mode trapped in the cavity.

$$\vec{E}_{mn}(x, y, z) = \vec{E}_0 H_m \left(\frac{\sqrt{2}x}{w(z)} \right) H_n \left(\frac{\sqrt{2}y}{w(z)} \right) \frac{w_0}{w(z)} \times \exp \left(-\frac{x^2 + y^2}{w(z)^2} \right) \exp \left(-ik \left(z + \frac{x^2 + y^2}{2r(z)} \right) + i(m+n+1)\psi(z) \right) \quad (15)$$

The frequency shift of a TEM_{mn} high-order mode relative to the TEM_{00} mode, at the same interference order, is given by[7]:

$$\Delta\nu_{mn} = (m+n) \frac{\nu_{\text{FSR}}}{\pi} \arccos \left(1 - \frac{l}{r_m} \right) = (m+n)\Delta\nu_t \quad (16)$$

where $\Delta\nu_t$ is the transverse mode spacing. Equation 16 implies that different cavity modes with the same $m+n$ overlapped with each other in the spectrum. The intensity distributions of the lowest modes are shown in figure 3.

If the cavity is close to rotational symmetric, Laguerre-Gaussian modes are supported by the cavity[9]. The Laguerre-Gaussian modes are labeled by radial index p and azimuthal index l . For simplicity, we label each Laguerre-Gaussian mode by L_p^l . The electric field distribution are given by:

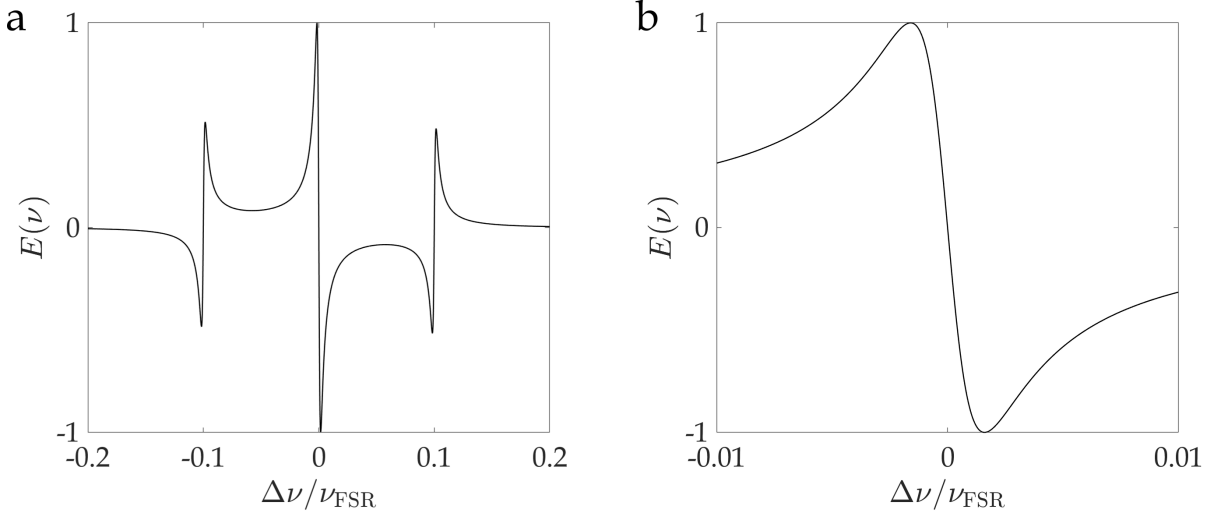


Figure 4: The error signal of parameters: $R = 0.99$, $T = 0.01$, and $\nu' = 0.1\nu_{\text{FSR}}$. (a) Overview of the error signal. Each sidebands also processes a sharp linear regime close to the frequency that one of the sidebands is on-resonance with the cavity. (b) The error signal at the vicinity of the resonance. The error signal is almost linear, which can be used for locking the laser to the cavity.

$$\vec{E}_{lp}(r, \phi, z) = \vec{E}_0 \frac{w_0}{w(z)} \left(\frac{r}{w(z)} \right)^{|l|} L_p^{|l|} \left(\frac{2r^2}{w(z)^2} \right) \times \exp \left(-\frac{r^2}{w(z)^2} \right) \exp \left(-ik \left(z + \frac{r^2}{2r(z)} \right) - il\phi + i(m+n+1)\psi(z) \right) \quad (17)$$

and the corresponding frequency shift is given by:

$$\Delta\nu_{lp} = (2p+l)\Delta\nu_t \quad (18)$$

The next-leading modes in the spectrum are TEM₀₁ and TEM₁₀ for the case of Hermite-Gaussian mode or L_0^1 for the case of Laguerre-Gaussian mode. Experimentally, we use the Laguerre-Gaussian mode L_0^1 as the indicator of perfect cavity rotational symmetry in the alignment progress (see section 4.2).

2.3 Pound-Drever-Hall Stabilization

The classical technique to lock a laser to a cavity is the Pound-Drever-Hall (PDH) laser frequency stabilization[5]. The PDH stabilization generates an error signal as a function of the laser detuning, which allows a stabilization on resonance with the optical resonator

Equation 6 shows that the cavity transmission is symmetric on the two sides of the transmission peak. To get an asymmetric error signal, we apply a phase modulation to the incoming laser. Assuming a small modulation parameter β , the laser includes a carrier and two frequency sidebands:

$$\begin{aligned} \tilde{E}_{\text{in}} &= \tilde{E}_0 \exp \left(i \left(2\pi\nu t + \beta \sin(2\pi\nu't) \right) \right) \\ &\approx \tilde{E}_0 \left(e^{2\pi i \nu t} + \beta e^{2\pi i (\nu+\nu')t} - \beta e^{2\pi i (\nu-\nu')t} \right) \end{aligned} \quad (19)$$

where ν and ν' are the carrier and modulation frequency, respectively.

The cavity reflection rate, as a function of frequency, is given by:

$$r_{\text{cav}}(\nu) = -\sqrt{R} \frac{1 - (R + T)e^{2\pi i\nu/\nu_{\text{FSR}}}}{1 - Re^{2\pi i\nu/\nu_{\text{FSR}}}} \quad (20)$$

The reflected field is given by:

$$\tilde{E}_r = \tilde{E}_0 \left(r_{\text{cav}}(\nu)e^{2\pi i\nu t} + \beta r_{\text{cav}}(\nu + \nu')e^{2\pi i(\nu + \nu')t} - \beta r_{\text{cav}}(\nu - \nu')e^{2\pi i(\nu - \nu')t} \right) \quad (21)$$

We measure the reflected power P_r :

$$P_r = \left| \tilde{E}_r \right|^2 \quad (22)$$

and extract the terms oscillating with the factor $\sin(2\pi\nu't)$ by demodulation:

$$P_r = 2\beta \left| \tilde{E}_0 \right|^2 \text{Im} \left(r_{\text{cav}}(\nu)r_{\text{cav}}^*(\nu + \nu') - r_{\text{cav}}^*(\nu)r_{\text{cav}}(\nu - \nu') \right) \sin(2\pi\nu't) + (\text{other frequency terms}) \quad (23)$$

The error signal is proportional to $E(\nu)$:

$$E(\nu) = \text{Im} \left(r_{\text{cav}}(\nu)r_{\text{cav}}^*(\nu + \nu') - r_{\text{cav}}^*(\nu)r_{\text{cav}}(\nu - \nu') \right) \quad (24)$$

As an example, we plot the function $E(\nu)$ for parameters: $R = 0.99$, $T = 0.01$, and $\nu' = 0.1\nu_{\text{FSR}}$ in figure 4. The error signal features a linear regime for the feedback control when the laser carrier is at the vicinity of cavity resonance, which allows us to stabilize the laser to the cavity resonance, as described in the cavity stabilization scheme.

3 Transfer Cavity Design

3.1 Optical Design

The high-reflectivity mirrors for the transfer cavity are PAN6345 partial reflector from Optoman, which have a intensity reflectivity $R = 99.95\% \pm 0.02\%$ at both 671 nm and 1064 nm for 0° incidence angle (see Appendix A for the summary of mirror properties). The reflecting surface has curvature $r_m = 1000$ mm with $\pm 1\%$ accuracy . The other surface is a flat surface and anti-reflection coated with the same wavelengths.

The length of the cavity is $l = 135$ mm, which is close to the first generation cavity. The free spectral range ν_{FSR} , linewidth Γ_c , finesse F , transverse mode spacing $\Delta\nu_t$, and the Gaussian mode waist radius w_0 of the cavity are:

$$\nu_{\text{FSR}} = 1.110 \text{ GHz} \quad (25)$$

$$\Gamma_c = 177 \text{ kHz} \quad (26)$$

$$F = 6.28 \times 10^3 \quad (27)$$

$$\Delta\nu_t = 186 \text{ MHz} \quad (28)$$

$$w_0 = 291 \mu\text{m} \quad (29)$$

The length of the cavity is fine-tuned by the Thorlab PA44M3KW piezo ring chip, which has a maximum displacement of $3.9 \mu\text{m} \pm 15\%$ at 150 V input voltage. For the 671 nm laser used in our experiment, the maximum displacement allows scanning over roughly 10 free spectral range.

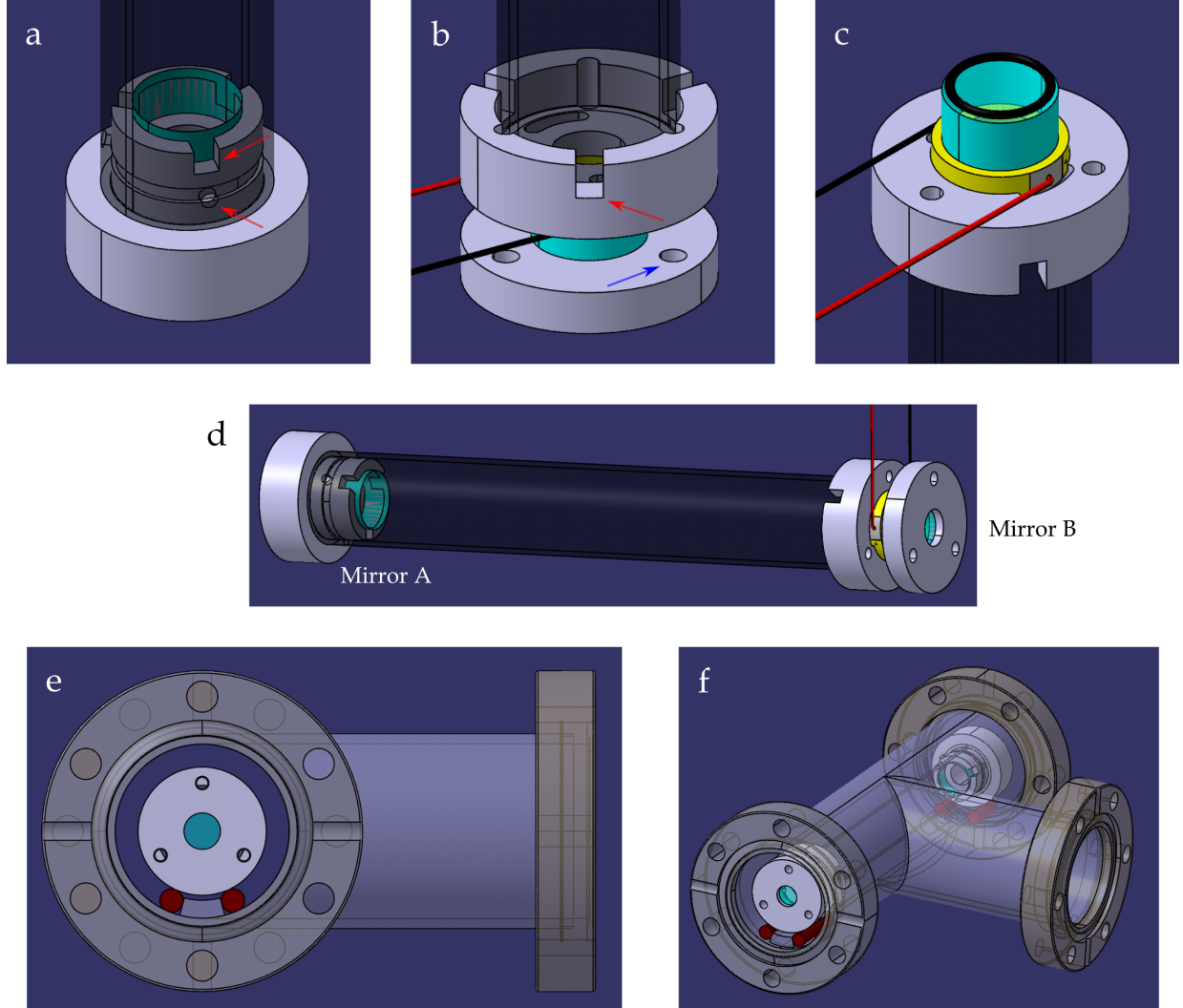


Figure 5: The mechanical design of the transfer cavity and its chamber. (a) Mirror A is glued to the holder by point gluings at the three cuts (upper red arrow) on the top. The CFRP tube (translucent black) is glued to the holder by point gluings at three holes (lower red arrow). (b) Mirror B is clamped to its holder and sandwiched by the piezoelectric ring and the rubber o-ring. The two holders are clamped by three screws (blue arrow, screws are hidden). The CFRP tube is glued to the holder by point gluings at the three cuts on the top (red arrow). (c) Detailed view of the o-ring, mirror B, and the piezoelectric driver on top of the holder. (d) Overview of the assembled transfer cavity. The two mirrors are labelled respectively. (e) Transfer cavity in the chamber. The two red rubber rods below are used for vibration damping. (f) Overview of the transfer cavity in the chamber. The port on the right is used for the cables.

3.2 Mechanical Design

The mechanical design of the transfer cavity includes the stainless steel cavity endcaps and carbon-fiber-reinforced polymers (CFRP) cavity body tube[10, 11]. The new transfer cavity will be enclosed by a chamber similar to the first generation transfer cavity such that we can change to the new cavity by simply replacing the chamber.

For simplicity in the texts below, we called the mirror which is glued to the stainless steel holder as mirror A, the other mirror as mirror B.

The stainless steel holders and the CFRP tube are designed to minimize the thermal expansion of the cavity. The CFRP has very low longitudinal thermal expansion coefficient: $\alpha_{\text{CFRP}} = (1 \sim 10) \times 10^{-7} / ^\circ\text{C}$. The thermal expansion of the tube is $(14 \sim 140) \text{ nm} / ^\circ\text{C}$ given the length of the cavity body tube is roughly 140 mm, which is almost negligible compared with the $3.9 \mu\text{m}$ maximum displacement of the piezo.

The stainless steel has a much higher thermal expansion coefficient: $\alpha_{\text{steel}} = (1.3 \sim 1.7) \times 10^{-5} / ^\circ\text{C}$. To eliminate the contribution to the total thermal expansion, we apply the tactic that the mirror A is placed inside the tube by the stainless steel holder, while the mirror B is placed outside so that the thermal expansion of the stainless steel is moving the two mirrors in the same direction. The thermal expansion of the piezo and the mirrors are all negligible.

Based on above, the transfer cavity is designed as follows (figure 5):

- The mirror A is directly glued to the stainless steel holder and the holder is glued to the CFRP tube. The stainless steel between the two gluing points (two red arrows in the figure 5(a)), which is 4 mm in thickness, will contribute to the thermal expansion by pushing the endcap and the cavity tube to opposite directions.
- The mirror B is sandwiched by the piezo ring and a rubber o-ring, which are in total clamped by another cap by 3 screws (figure 5 (b)(c)). The rubber o-ring will act as a spring to keep the mirror touching the piezo ring. The CFRP tube is similarly glued to the cavity holder. The thickness of the stainless steel between the gluing point and the bottom of the piezo ring are set to be 4 mm to cancel out the thermal expansion.
- The assembled cavity will be directly positioned in a chamber (figure 5 (e)(f)). Four rubber rods hold the cavity from the bottom for vibration damping and keep the cavity concentric to the chamber window. The third port of the chamber is used for the electric connections. The chamber will be sealed to completely get rid of humidity and pressure changes and minimize temperature fluctuations. But the chamber will not be pumped to vacuum for simplicity.

4 Experimental Implementation

4.1 Cavity Characterization Setup

The cavity is tested at 1064 nm wavelength throughout the experiment. The laser used is Orange One Single Frequency CW Fiber Laser from MenloSystems, which has a linewidth $< 100 \text{ kHz}$ at a measurement duration of $120 \mu\text{s}$. The laser linewidth is roughly a half of the cavity linewidth, which will lead to broadening in the transmission spectrum. The laser linewidth are all taken into account in the subsequent measurements.

The laser passes through the iXblue NIR-MX-LN-10 amplitude modulator for tuning its power and generating sidebands as frequency calibrations. Two mirrors and two lenses are used to couple the laser beam to the TEM_{00} mode of the cavity. The two mirrors are used to tune the tilting of the laser beam. Here, the beam waist of the fiber output port is $3.3 \mu\text{m}$, which is a standard for optical fiber at 1064 nm wavelength. A

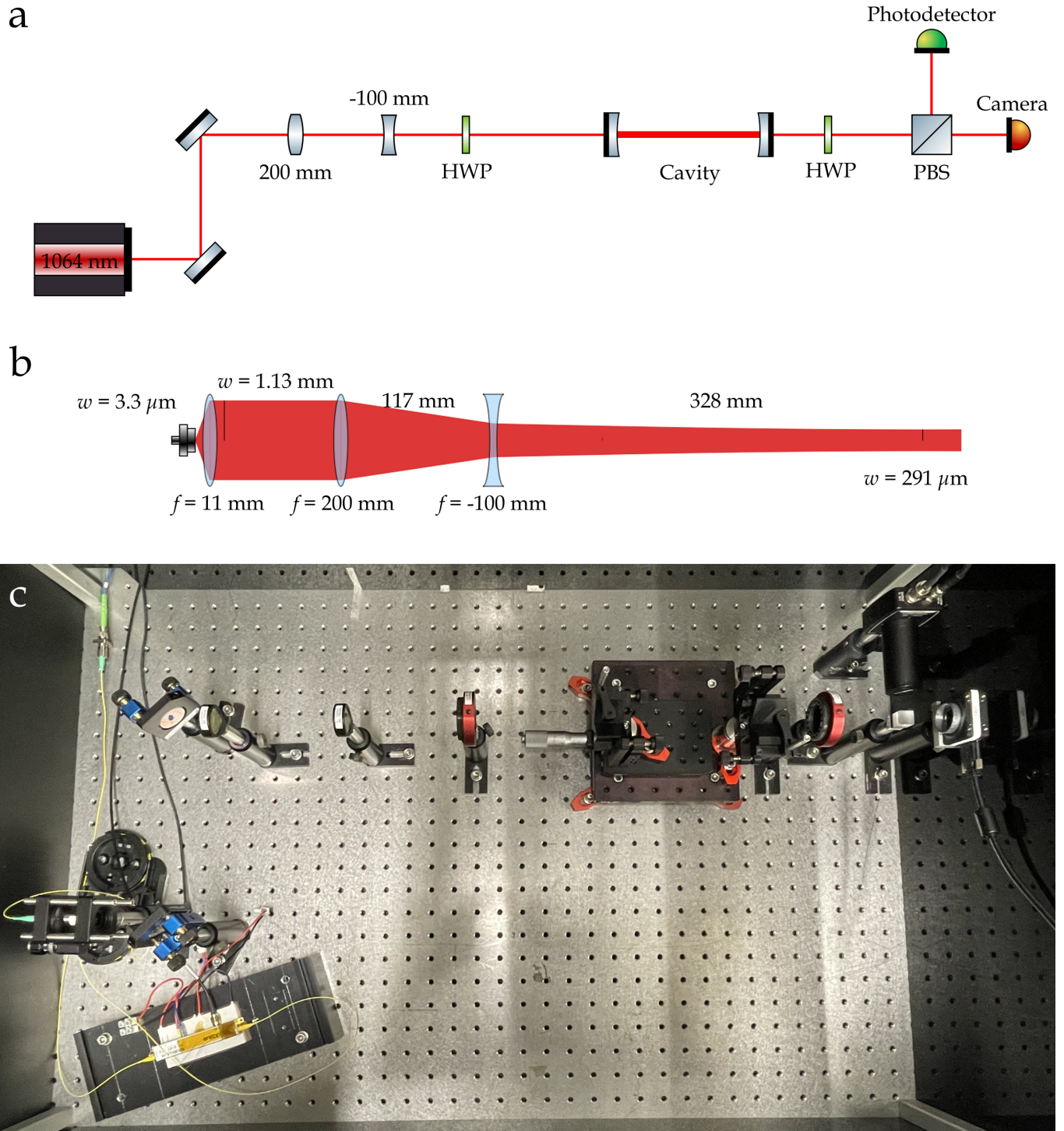


Figure 6: (a) Schematic of the testing setup. HWP: half-wave plate. PBS: polarized beam splitter. (b) Schematic of the laser beam propagation, including the position of all the lenses for coupling the laser to the cavity mode. (c) The photo of the testing setup. At the left bottom corner is the amplitude modulator.

lens with 11 mm focal length collimates the laser beam. The collimated laser has a beam waist of 1.13 mm. To make the laser beam coincide with the TEM_{00} cavity mode, we use a convex lens and a concave lens to form a Galileo telescope, which focus the laser beam to the size of the waist $w_0 = 291 \mu\text{m}$ at the center of the cavity. All of the Gaussian beam operations are simulated by the software GaussianBeam[12]. The position of the lenses are shown in figure 6(b).

The two mirror and cavity endcap assemblies are held by two V-shaped holders. One of the cavity endcap stands on the translational stage for fine-tuning the distance between the two mirrors. Both endcaps stand on a smaller breadboard to mitigate the vibration noise. The two half-wave plates (HWP) are used to change the incoupling beam polarization and split the power between the photodetector and the camera. The camera records the shape of the cavity modes and the photodetector measures the transmission spectrum.

4.2 Cavity Assembling and Alignment

Before assembling the cavity, we tested the finesse of three pairs of mirrors. The pair with the highest finesse is selected to be assembled. The assembling and alignment are performed by the steps described as follows.

Assemble the mirrors to the stainless steel holders

The two bare mirrors are firstly assembled to the endcaps. The Araldite RAPID epoxy glue is used in all the gluing steps. Mirror A is directly glued to its holder. Mirror B is sandwiched by the piezo chip and the rubber o-ring. Three screws clamp the assembly together (figure 7 (a)(b)).

After assembling, both endcaps are clamped to the V-shape holders. Both V-shape holders have horizontal and vertical tilting tunability for the next alignment steps (figure 7 (c)).

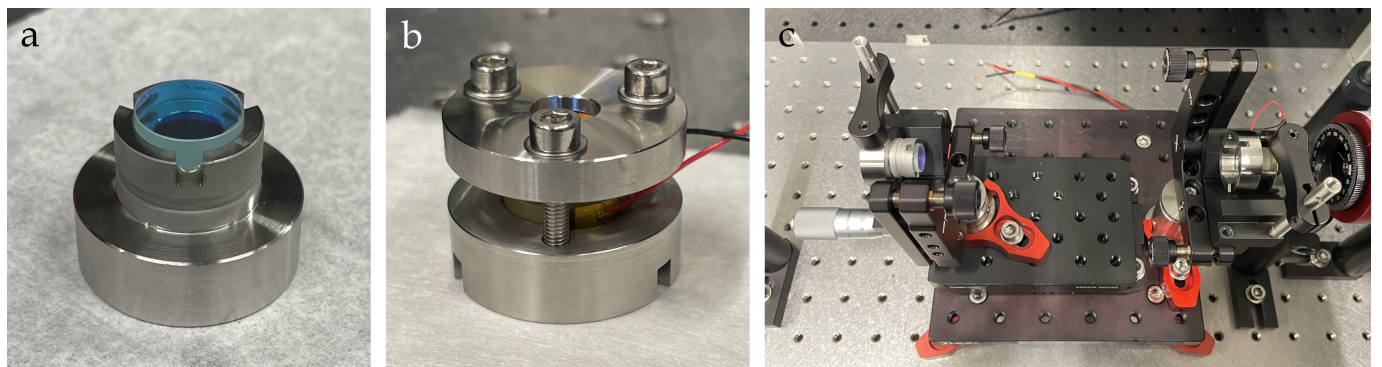


Figure 7: Assemble the mirrors to the stainless steel holders. (a) Mirror A glued to the stainless steel holder. (b) Mirror B clamped to the stainless steel parts by three screws. The cable in the figure is the piezo driving cable. (c) Cavity mirrors assembled to the corresponding stainless steel holder. Both stainless steel holders are clamped to the V-shaped holder for alignment.

Aligning the cavity mirrors

Aligning the cavity mirrors includes 2 criterias:

- The cavity modes are located at the center of both cavity mirrors.
- The center of the two cavity mirrors are parallel.

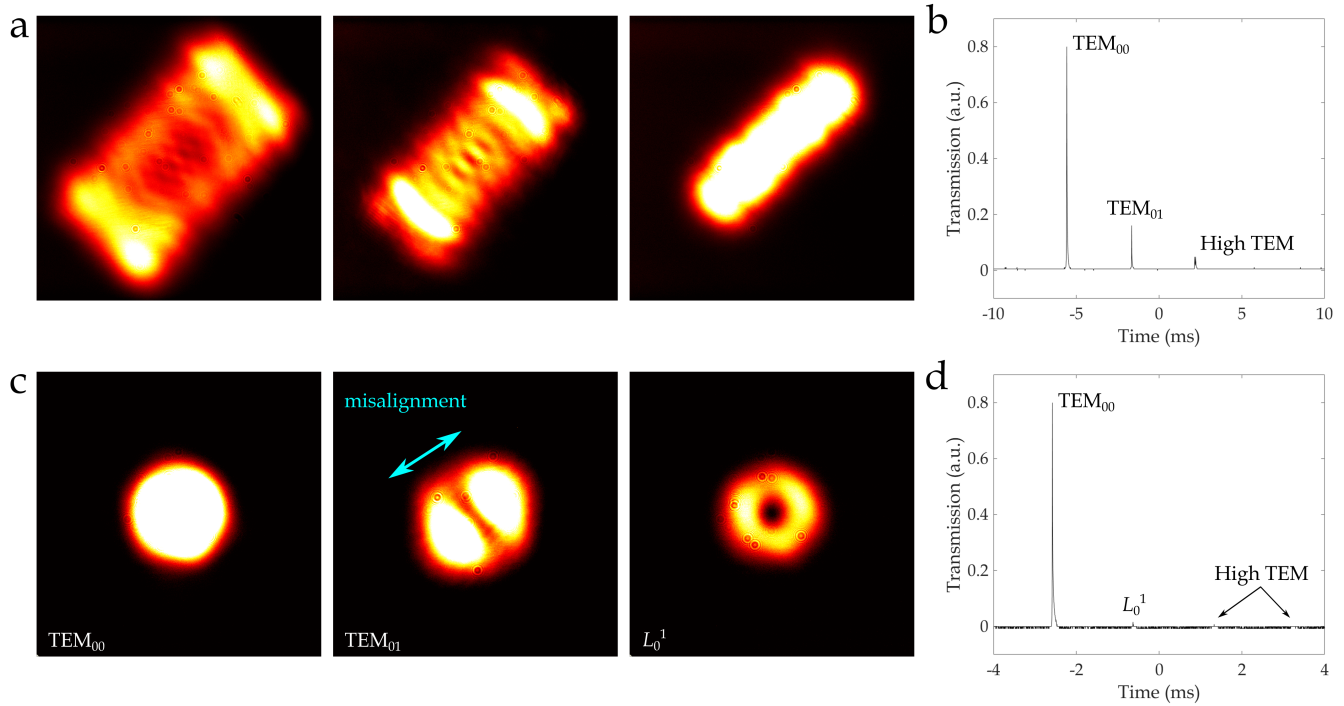


Figure 8: (a) Typical transmission pattern of the cavity after the course alignment. The pattern is a superposition of multiple cavity modes, indicating many high-order modes are coupling to the laser. From left to right, the transmission pattern is getting smaller, indicating the cavity is better aligned that the laser couples to smaller low-order modes. (b) Typical transmission spectrum after the fine alignment. The first few peaks are labeled with the corresponding modes. (c) The transmission pattern of the TEM₀₀, TEM₀₁ and L_0^1 modes. The TEM₀₁ mode indicates the misalignment direction of the cavity mirrors, as shown by the blue arrow. The L_0^1 mode is almost rotationally symmetry. (d) Typical transmission spectrum after the final optimization. The spectrum shows that the TEM₀₀ is almost the unique mode coupled to the laser.

The cavity alignment follows the procedures below:

- Incoupling laser preparation: Before putting the mirrors on the V-shaped holders, align the incoming laser so that the laser passes through the expected center position of both mirrors. The position of the incoupling laser will be kept almost unaltered in the following steps, guaranteeing that the cavity modes are centered to the mirrors.
- Coarse alignment: Put the mirror B to the V-shaped holder firstly and adjust its back reflection to coincide with the incoming laser. In the figure 7 (c), the laser is travelling from left to right and the mirror B is the right one. Then put the mirror A to the V-shaped holder. Scan the incoming laser frequency by one free spectral range at 100 Hz. In this case, all the cavity modes can be transmitted through the cavity at one certain frequency. Tilt mirror A so that some transmission signal are observed at the camera. The cavity is usually coupled to some high order modes at this moment. The typical image captured by the camera is shown in figure 8 (a), which is a superposition of several high order modes.
- Fine alignment: To further couple the incoming laser to the low order modes, we fine tune the tilting of the two mirrors such that the laser is coupling to smaller cavity modes. Figure 8 (a) shows the typical image at the camera, and from left to right the transmission images are coupling to lower order

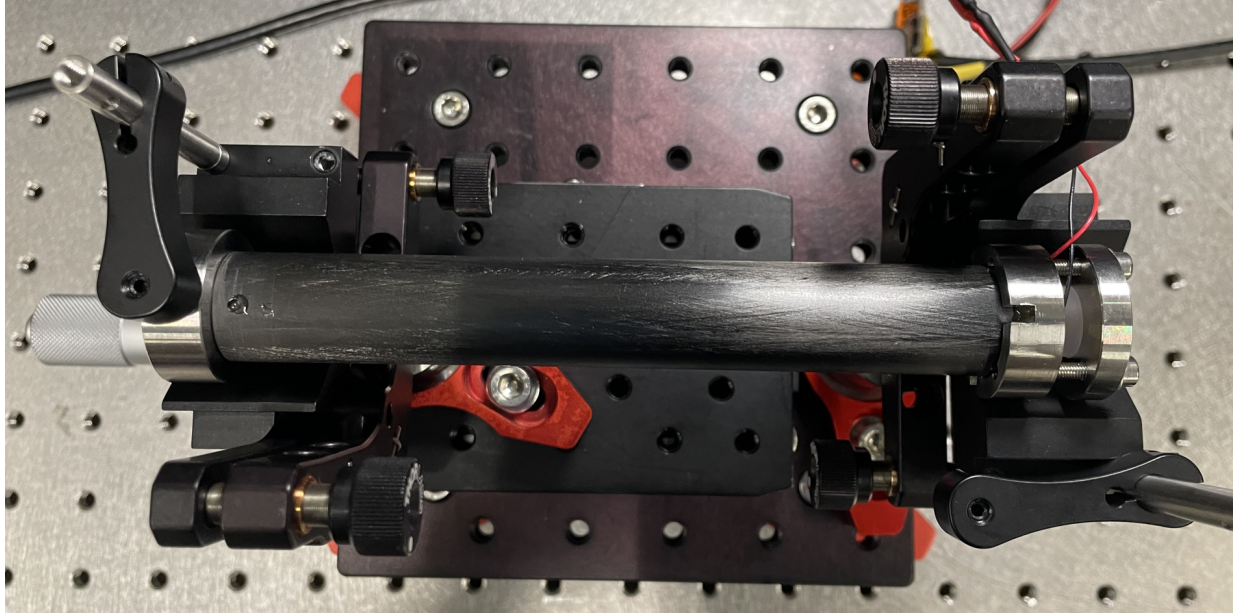


Figure 9: Top view of the cavity, after assembling the stainless steel holders to the CFRP tube. The glue is put on the holes (left) and the cuts (right).

modes. Figure 8 (b) shows the typical transmission spectrum with different peaks distinguished at the end of the fine alignment stage. The TEM_{00} mode is expected to be the dominant one.

- Final optimization: This stage is aiming for perfect rotational symmetry. We assume that the incoupling laser is a perfect Gaussian beam and use it as a reference. The goal is making the TEM_{00} mode the unique one that the incoming laser coupled to the cavity. The optimization includes the following steps.

Fine tune the incoupling lens before the cavity such that all High TEM modes except TEM_{00} and TEM_{01} are negligible.

Narrow down the frequency scanning range, such that the laser frequency is only scanning over the TEM_{00} or TEM_{01} mode. The shape of the TEM_{01} mode shows the misalignment direction of the cavity mirrors (the blue arrow in the figure 8 (c)). Further fine tune the tilting of the mirrors to reduce the coupling of the TEM_{01} mode.

The fine tuning process finally ends when the TEM_{01} mode becomes the L_0^1 Laguerre-Gaussian mode, indicating perfect rotational symmetry. Usually, its intensity is very faint that the transmission spectrum includes exclusively the TEM_{00} mode (figure 8 (d)).

Assemble the stainless steel holders to the CFRP tube

After the alignment, the CFRP tube is inserted between the two stainless steel holders. The alignment remains good after the insertion. Then, a little drop of glue is put at the holes or cuts reserved for gluing. Both of the endcaps are clamped during the process of glue curing. The clamps are removed after the gluing. At this stage, the alignment of the cavity is completed and remains good in the following characterizations.

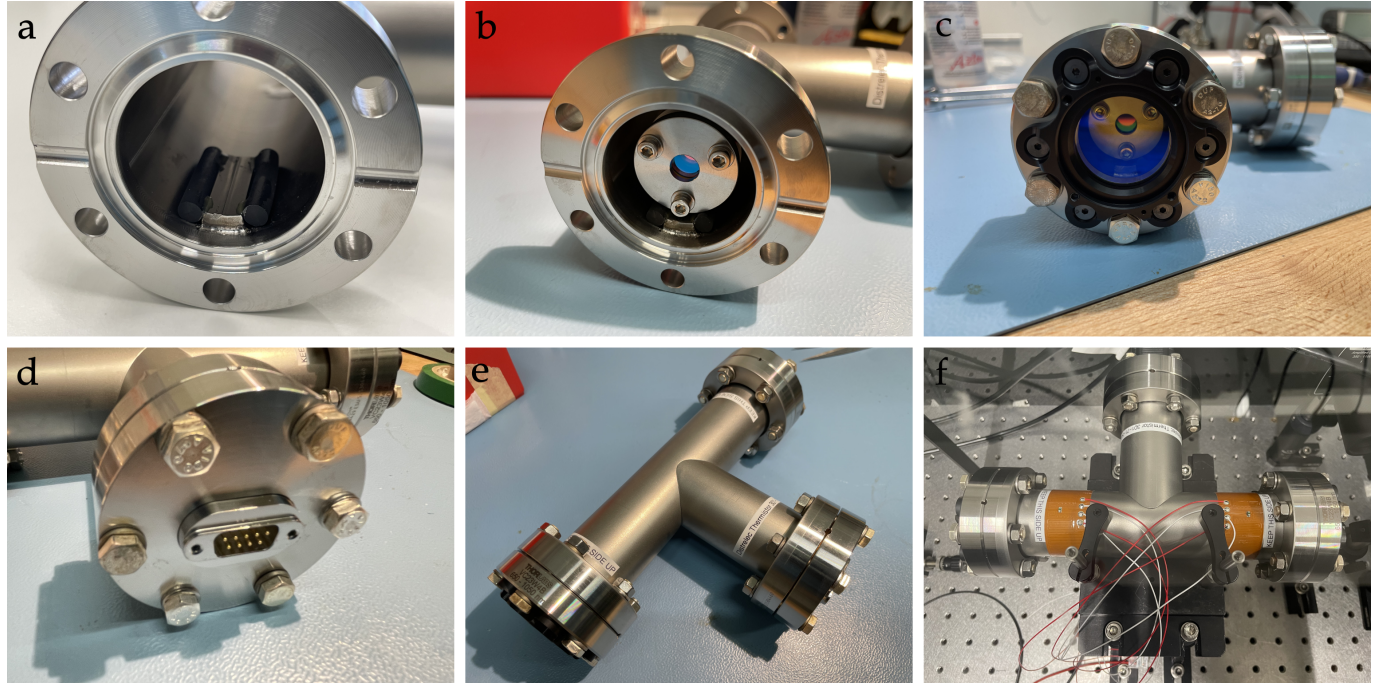


Figure 10: (a) The vibration-damping rubber rods glued to the separator. The separator is welded to the chamber. (b) The cavity inside the chamber, which stands on top of 4 vibration-damping rubber rods. (c) The viewport with cavity inside of the sealed chamber. (d) The 9-pin plug for electric connection of the piezo driver and the thermistor. (e) Overview of the sealed chamber. (f) The top view of the chamber with two foil heaters glued to it.

Assemble the cavity and the chamber

The cavity is sealed in a chamber. The chamber is used for mitigating the cavity resonance drift due to changes in temperature, humidity, and atmospheric pressure. The cavity stands on top of 4 vibration-damping rubber rods, which are glued to a separator inside the chamber. The separator is welded to the chamber. A thermistor is installed inside the chamber to measure the interior air temperature of the cavity. Two Thorlab HT10K foil heater are glued on the two arms of the chamber outer surface for temperature regulation, see figure 10 (f).

5 Cavity Parameters Characterization

5.1 Cavity Spectrum

We measure the cavity transmission spectrum by scanning the input laser frequency. The input laser is amplitude-modulated at 100 MHz. The 2 sidebands at 100MHz are used for calibration of the frequency scanning rate. We assume that the laser frequency is scanned linearly with respect to time. Therefore, the free spectral range is given by:

$$\nu_{\text{FSR}} = 1.10 \text{ GHz} \quad (30)$$

which is close to the theoretically predicted value 1.11 GHz given by the cavity length of 135 mm. To estimate the nonlinearity of the laser frequency scanning, we compare the time gap between the carrier and the sideband in different interference orders. The time gap differs by 6% for the two interference

orders shown in figure 11 (a), which can be considered as an estimate of the uncertainty of the measured free spectral range.

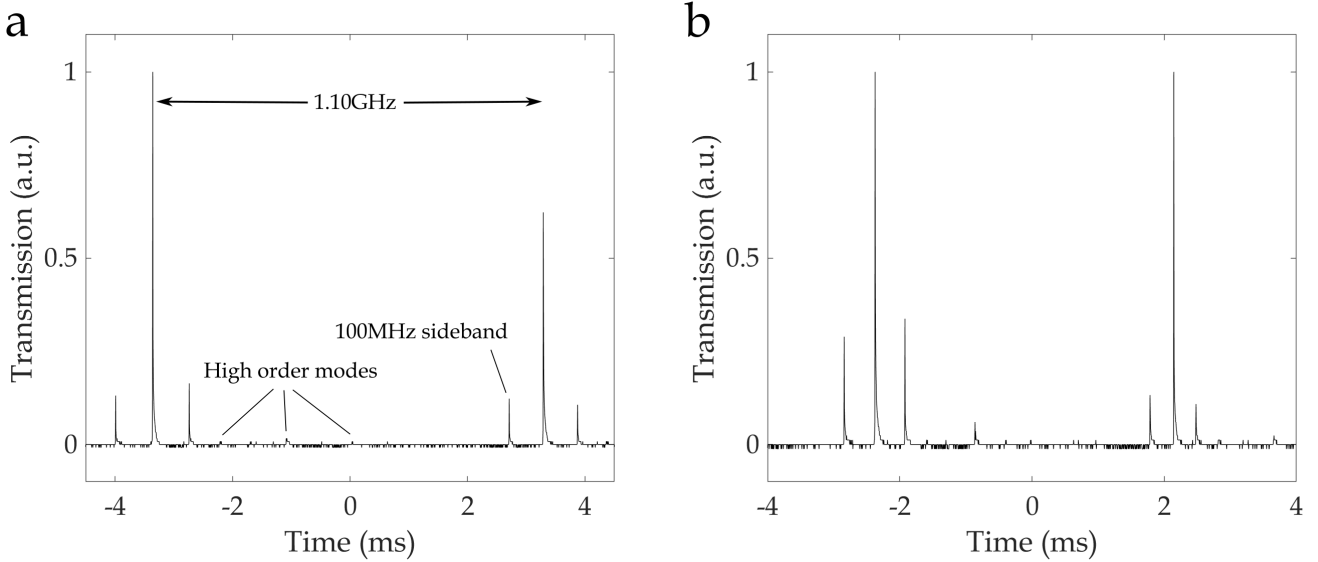


Figure 11: The cavity transmission spectrum with scanning (a) the laser frequency and (b) the cavity resonance frequency by the piezo. The input laser is amplitude-modulated at 100 MHz, creating a pair of sideband with a known frequency as a calibration. All remaining high-order modes are negligible in the spectrum.

The transmission spectrum is also observed by scanning the cavity piezo voltage, which changes the cavity resonance frequency. The cavity piezo features a much higher nonlinearity since the two time gaps differ by $\approx 30\%$ in the figure 11 (b). In all the following spectral measurements, laser frequency scanning are applied to reduce the affect of the nonlinearity.

5.2 Cavity Finesse and Transmission

We extract the cavity finesse by scanning the laser frequency and measure the transmission linewidth. Here, we take into account that the laser linewidth is roughly a half of the cavity linewidth, which results in the transmission linewidth broadening. We model the broadening by assuming the laser spectrum is Gaussian with full-width half-maximum (FWHM) Γ_l . The intensity spectrum of the laser $I(\nu)$ is proportional to:

$$I(\nu) \propto \exp\left(-(4 \log 2) \times \frac{(\nu - \nu_l)^2}{\Gamma_l^2}\right) \quad (31)$$

where ν_l is the laser center frequency.

The intensity transmission rate of the cavity is given by equation 6. Here we rewrite it as:

$$T_{\text{cav}}(\nu) = \frac{T_c}{1 + \left(\frac{2\Delta\nu}{\Gamma_c}\right)^2} \quad (32)$$

where T_c is the peak cavity transmission and Γ_c is the cavity linewidth.

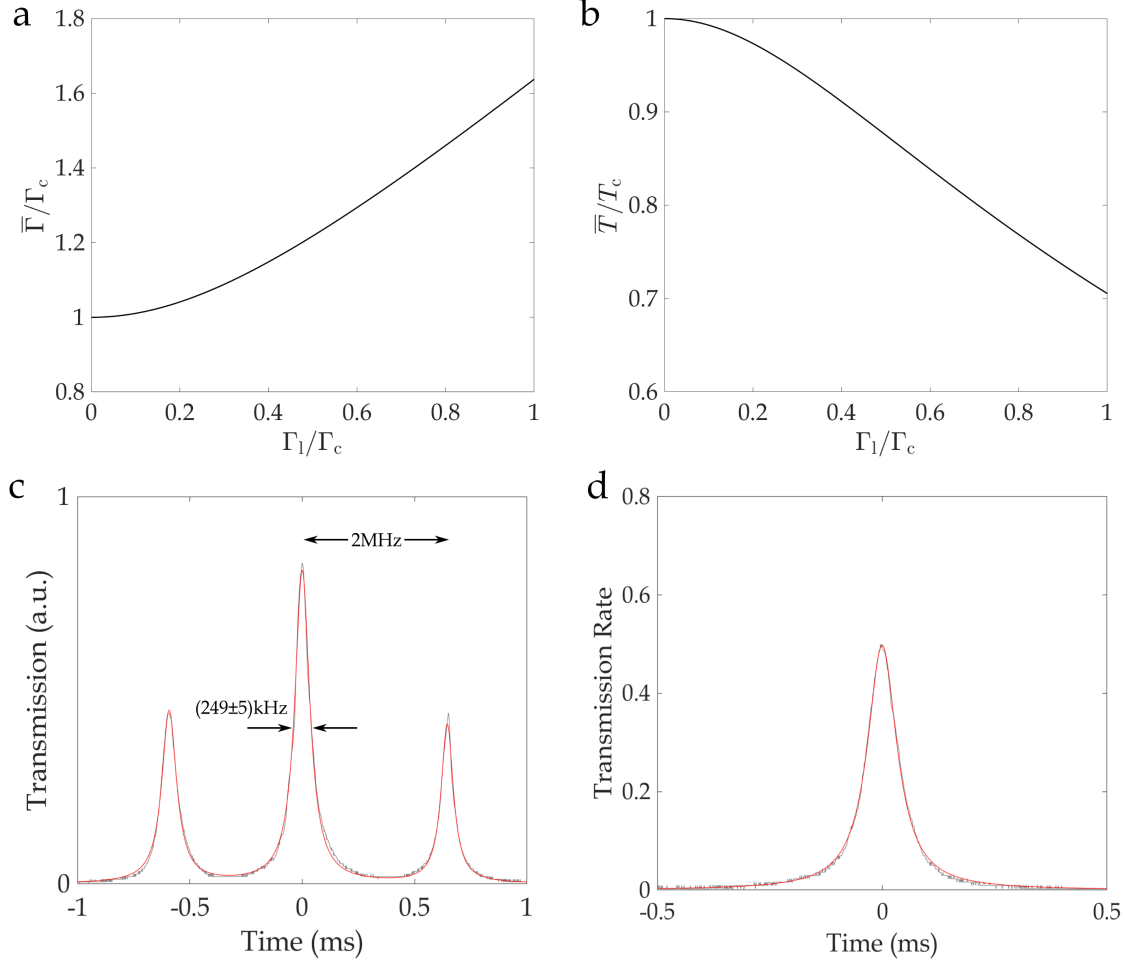


Figure 12: (a) The observed linewidth and (b) the observed peak transmission due to the finite laser linewidth, normalized by the cavity linewidth Γ_c or peak cavity transmission T_c . (c) The transmission spectrum measurement with two 2 MHz sidebands. The red line corresponds to a triple-Lorentzian fit. (d) Transmission rate measurement, fitted by a Lorentzian function.

The observed spectrum is a convolution of equation 31 and 32, which is generally known as Voigt profile. We plot the observed linewidth $\bar{\Gamma}$ and the observed peak transmission \bar{T} in figure 12 (a) and (b). Here, the observed transmission linewidth $\bar{\Gamma}$ is defined as the FWHM of the spectrum.

The transmission linewidth $\bar{\Gamma}$ is measured by applying a 2 MHz modulation as frequency calibration (figure 12 (c)). In sufficiently small scanning range, the laser frequency features very low non-linearity. The transmission spectrum is fitted by a triple-Lorentzian function. The measurements are repeated for 10 times and the averaged $\bar{\Gamma}$ is given by:

$$\bar{\Gamma} = (249 \pm 5) \text{ kHz} \quad (33)$$

The peak transmission \bar{T} is given by the ratio of the maximum transmitted power and the input power of the cavity (figure 12 (d)).

$$\bar{T} = (49.9 \pm 0.5)\% \quad (34)$$

where the maximum transmitted power is measured by a calibrated photodetector.

The $\bar{\Gamma}$ and \bar{T} given above correspond to the worst case for the cavity that the laser linewidth is essentially considered to be zero. To give an estimate for the best case, we choose the laser linewidth to be its upper bound: $\Gamma_c = 100 \text{ kHz}$. Using the numerical curves given by figure 12 (a) and (b), we obtain:

$$\Gamma_c = (206 \pm 6) \text{ kHz} \quad (35)$$

$$T_c = (56.7 \pm 0.7)\% \quad (36)$$

Equation (33) to (36) give the upper and lower bound of the cavity linewidth and peak cavity transmission. The range of the finesse F given by the range of the linewidth and the free spectral range is:

$$F = (4.42 \sim 5.34) \times 10^3 \quad (37)$$

The theoretical finesse F_{theo} given by equation 8 is:

$$F_{\text{theo}} = (6.3^{+4.2}_{-1.8}) \times 10^3 \quad (38)$$

where we used the intensity reflectivity of the mirror is $R = (99.95 \pm 0.02)\%$.

The experimental finesse agrees with the spec sheet of the mirror, which also satisfies the experimental requirement.

5.3 Cavity Thermal Stability

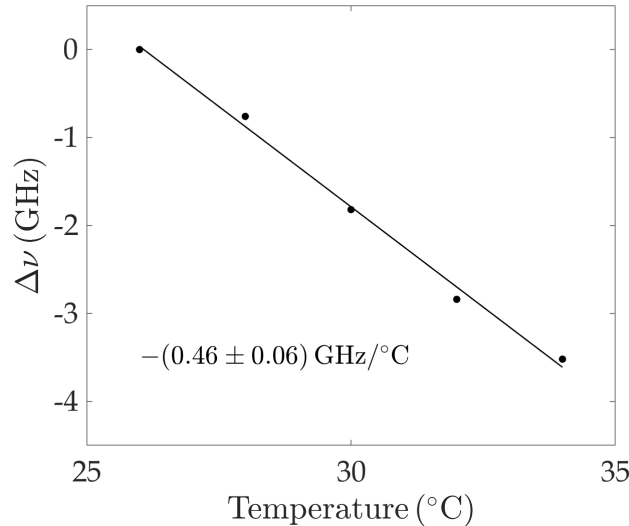


Figure 13: Cavity resonance frequency drift $\Delta\nu$ as a function of temperature.

The cavity spacer tube is made of CFRP which features extremely low thermal expansion. Here, we measure the thermal cavity resonance shift by actively control the interior temperature of the chamber. We apply the Meerstetter Engineering TEC-1091 temperature controller to drive two foil heaters. The laser is locked to the cavity resonance by the side-of-fringe locking by Red Pitaya and software package PyRPL[13]. A HighFinesse WS6 wavemeter monitors the laser frequency with a absolute accuracy $\sim 100 \text{ MHz}$ and providing a relative frequency resolution of $< 10 \text{ MHz}$.

We measure the cavity resonance shifting $\Delta\nu$ in the temperature range of $25 \sim 35^\circ\text{C}$. A linear fit shows that the resonance drifting is:

$$\frac{\Delta\nu}{\Delta T} = -(0.46 \pm 0.06) \text{ GHz}/^\circ\text{C} \quad (39)$$

The coefficient of thermal expansion α_T , defined as the relative expansion of the cavity length, is given by:

$$\alpha_T = -\frac{\Delta\nu}{\Delta T} \frac{\lambda}{2\nu_{\text{FSR}} l} = -\frac{\Delta\nu}{\Delta T} \frac{\lambda}{c} = (1.6 \pm 0.2) \times 10^{-6}/^\circ\text{C} \quad (40)$$

where we have used the length of the cavity $l = 135 \text{ mm}$.

The coefficient of thermal expansion is slightly higher than the bare CFRP tube ($(0.1 \sim 1) \times 10^{-6}/^\circ\text{C}$). It is similar to the ETH transfer cavity described in the Master thesis by Lorenz Hruby ($1.7 \times 10^{-6}/^\circ\text{C}$), which uses the same material as the cavity body[10]. The potential limitation of reducing the coefficient of thermal expansion can be the high thermal expansion of the epoxy glue. The typical size of the glue is 1 mm but the thermal expansion is $(5 \sim 8) \times 10^{-5}/^\circ\text{C}$ for epoxy glue. Therefore, the thermal expansion contributed by the glue is comparable to the whole CFRP tube, which increases the overall thermal expansion.

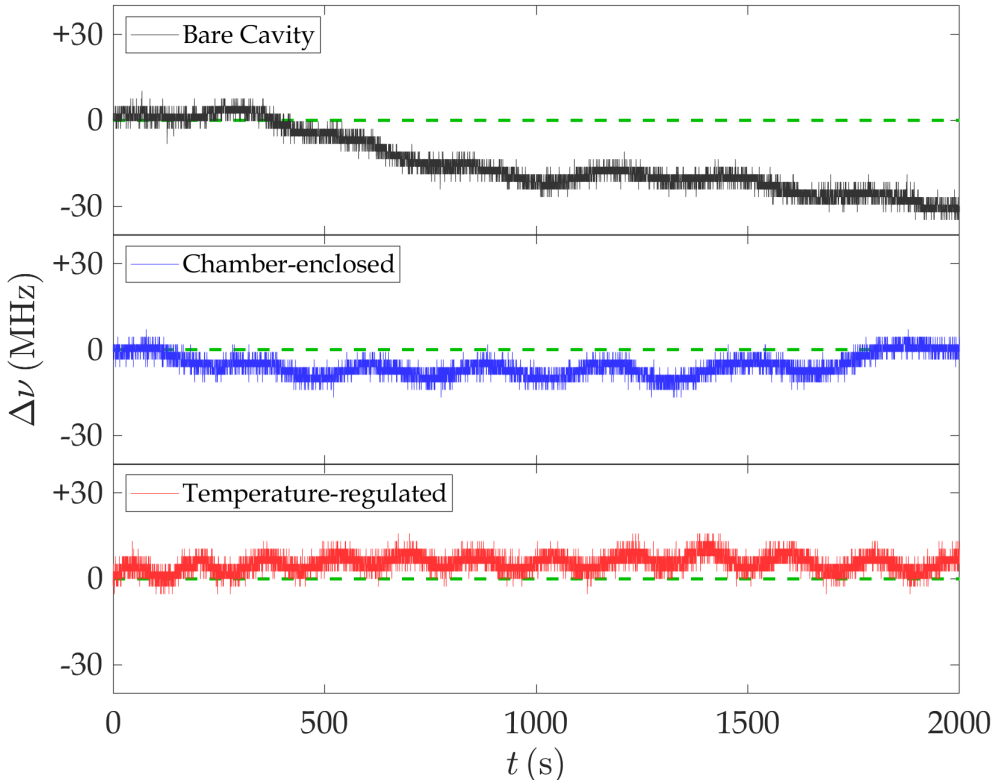


Figure 14: The cavity resonance frequency as a function of time for the bare cavity, the chamber-enclosed cavity and the temperature-regulated cavity. The green dashed lines are showing the origin of the frequency drift. The trend of the lines show the resonance drift due to the cavity thermal expansion. The wiggles are suspected to be the noise of the wavemeter.

The cavity thermal stability is significantly improved with the temperature controller compared with the bare cavity in the air. In the usual operating condition, the temperature controller is able to stabilize the

air temperature of the chamber within $0.01\text{ }^{\circ}\text{C}$, which results in a 5 MHz drift of the resonance frequency. Here, we monitor the stability of the cavity resonance by locking the laser to the cavity resonance and monitor the laser frequency. The thermal stability gets improved when the cavity is sealed inside the chamber, and further improved if the temperature regulation is applied. The cavity resonance maintains stable up to a few MHz, which agree with the typical temperature fluctuation of the chamber.

It is worth to point out that all the laser frequency measurements here go beyond the absolute accuracy of the wavemeter. The regular wiggling in figure 14 is suspected to be the internal noise of the wavemeter. The stability measured here can only be roughly considered as a drifting of the relative frequency at a time scale of an hour. But it is sufficiently persuasive to show that the temperature regulation significantly improved the temperature stability compared with the bare cavity.

6 Conclusion and Outlook

We presented the design of the second generation transfer cavity. The new design exhibits the following features:

- High finesse and transmission. The finesse of the cavity reaches roughly 5×10^3 , which is sufficient for the stabilization chain. The transmission reaches $> 50\%$, allowing the cavity to be utilized as a frequency filter.
- High thermal stability. The thermal expansion coefficient of the cavity reaches as low as $1.6 \times 10^{-6}/^{\circ}\text{C}$, which is close to the thermal expansion coefficient of a bare CFRP tube. With the temperature controller, the cavity temperature can be stabilized to $0.01\text{ }^{\circ}\text{C}$ in the usual operating condition, which corresponds to only a 5 MHz frequency drift.
- Simple and cost-effective. The new design has reasonably high finesse and transmission with only mirrors at 99.95% intensity reflectivity, which can be fabricated by the standardized mirror coating techniques. The mirror holders and cavity spacer are all easy to fabricate in a mechanical workshop. All assembling steps are designed to be effortless.

The new transfer cavity will be installed to the cavity QED experiment to improve the thermal stability. In the future experiment, more similar cavities will be applied as high-precision frequency filters to separate spatially overlapped laser beams with close frequencies, e.g. the carrier and sidebands of a phase-modulated laser. The simple and cost-effective design paves the way of achieving the goal without massive investment.

References

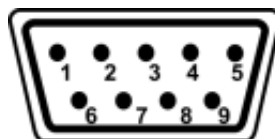
- [1] Helson V. Frequency stabilization and narrowing of lasers on a Fabry-Pérot cavity. 2017: 39.
- [2] Roux K. Cavity Quantum Electrodynamics with strongly correlated fermions. 2022: 249. <http://info.science.epfl.ch/record/291438>. DOI: <https://doi.org/10.5075/epfl-thesis-8282>.
- [3] Ketterle W Zwierlein M W. Making, probing and understanding ultracold Fermi gases. *La Rivista del Nuovo Cimento*, 2008, 31: 247-422.
- [4] Mivehvar F, Piazza F, Donner T. Cavity QED with quantum gases: new paradigms in many-body physics. *Advances in Physics*, 2021, 70(1): 1–153. <http://dx.doi.org/10.1080/00018732.2021.1969727>. DOI: 10.1080/00018732.2021.1969727.

- [5] Black E. An introduction to Pound-Drever-Hall laser frequency stabilization. *American Journal of Physics*, 2001, 69(1): 79-87. eprint: https://pubs.aip.org/aapt/ajp/article-pdf/69/1/79/10115998/79__1__online.pdf. <https://doi.org/10.1119/1.1286663>. DOI: 10.1119/1.1286663.
- [6] Helson V. Many-body physics with strongly interacting fermions coupled to light. 2023: 180. <http://infoscience.epfl.ch/record/302108>. DOI: <https://doi.org/10.5075/epfl-thesis-9589>.
- [7] Bachor H Ralph T. A guide to experiments in quantum optics. c2019.
- [8] Siegman A. Lasers. 1986.
- [9] Kogelnik H Li T. Laser beams and resonators. *Applied optics* (2004), 1966, 5(10): 1550-1567.
- [10] Lorenz H. Towards a 3D optical lattice potential inside an optical high-finesse cavity. 2013: 99.
- [11] Zwettler T. Suppression of heating mechanisms for deep optomechanical ground-State cooling. 2019: 109.
- [12] GaussianBeam. (2007-06-23). <https://sourceforge.net/projects/gaussianbeam/>.
- [13] Neuhaus L, Metzdorff R, Chua S, PyRPL (Python Red Pitaya Lockbox) — An open-source software package for FPGA-controlled quantum optics experiments//2017 Conference on Lasers and Electro-Optics Europe, European Quantum Electronics Conference (CLEO/Europe-EQEC). 2017: 1-1. DOI: 10.1109/CLEOE-EQEC.2017.8087380.

A Properties of the Cavity Mirror

	Surface 1	Surface 2
671 nm, 0° incidence	Partial reflect $R = 99.95\% \pm 0.02\%$	Anti-reflect $R < 0.2\%$
1064 nm, 0° incidence	Partial reflect $R = 99.95\% \pm 0.02\%$	Anti-reflect $R < 0.1\%$
Radius of curvature	−1000 mm ($\pm 1\%$)	FLAT

B Connection Diagram of the Sub D-9 Connector to the Chamber



Pin Number	1~2	3~7	8	9
Connection	Thermistor	None	Pizeo (+)	Pizeo (-)

Thermistor: Distrelec 301-71-547